Science of the Total Environment 691 (2019) 969–980

Contents lists available at ScienceDirect

Science of the Total Environment

journal homepage: www.elsevier.com/locate/scitotenv

A comprehensive understanding of enhanced Pb mobilization in sediments caused by algal blooms

Qin Sun [a], Juan Lin [b,c,1], Shiming Ding [b,*], Shuaishuai Gao [b,c], Mingrui Gao [a], Yan Wang [b,d], Chaosheng Zhang [e]

[a] Key Laboratory of Integrated Regulation and Resource Development on Shallow Lakes, Ministry of Education, College of Environment, Hohai University, Nanjing 210098, China
[b] State Key Laboratory of Lake Science and Environment, Nanjing Institute of Geography and Limnology, Chinese Academy of Sciences, Nanjing 210008, China
[c] University of Chinese Academy of Sciences, Beijing 100049, China
[d] Nanjing EasySensor Environmental Technology Co., Ltd, Nanjing 210018, China
[e] International Network for Environment and Health, School of Geography and Archaeology and Ryan Institute, National University of Ireland, Galway, Ireland

HIGHLIGHTS

- Mobile Pb was studied using high-resolution techniques in eutrophic lake sediment.
- Soluble Pb concentrations in overlying water in summer and autumn exceeded EPA-CMC.
- Fe/Mn oxide reduction and DOC complexation induced high Pb mobility in summer.
- Algal bioaccumulation and decomposition induced high Pb mobility in autumn.

GRAPHICAL ABSTRACT

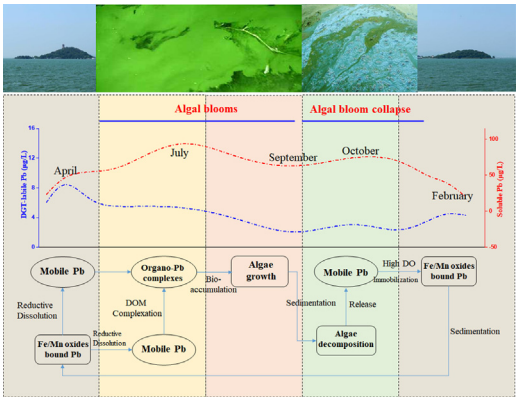

ARTICLE INFO

Article history:
Received 16 June 2019
Received in revised form 9 July 2019
Accepted 10 July 2019
Available online 11 July 2019

Editor: Daniel CW Tsang

Keywords:
Sediment
Eutrophic lake
Lead
Risk assessment
Dissolved organic matter

ABSTRACT

A good understanding of lead (Pb) mobilization in eutrophic lakes is a key to the accurate assessment of Pb pollution. In this work, dissolved and labile Pb was determined by both high resolution dialysis (HR-Peeper) and diffusive gradients in thin films (DGT) in sediment-water profiles of the hyper-eutrophic Meiliang Bay of Lake Taihu on a monthly basis during one year. The drinking water standards for dissolved Pb of the World Health Organization (10 μg/L) and those of China were exceeded in the overlying water (20.79–118.5 μg/L). Out of which, a total of five months even exceeded the fisheries water quality limitation (50 μg/L) in China. The algal blooms created an anaerobic environment in the surface sediments in July. The reductive conditions led to the dissolution of Fe/Mn and this caused the release of Pb, followed by organic matter complexation. This was supported by the coincident changes of dissolved Pb with dissolved organic matter (DOM) in sediments under anaerobic incubation. Algae residue decomposition in October caused another distinct release of Pb, but this process should be considerably suppressed by increased sulfide precipitation and pyrite adsorption of Pb ion. These results indicated that Pb mobilization in sediments can be significantly enhanced by algal blooms in eutrophic lakes, indicating that further attention should be paid to Pb pollution in waters with harmful algal blooms.

* Corresponding author.
E-mail address: smding@niglas.ac.cn (S. Ding).
[1] Co-first author.

https://doi.org/10.1016/j.scitotenv.2019.07.152
0048-9697/

1. Introduction

Lead (Pb) is one of the most toxic metals causing neurological, hematological, gastrointestinal and reproductive pathologies of animals (Garcia-Leston et al., 2010). Anthropogenic activities, such as mining, smelting, burning of coal, battery manufacturing and metal plating, have led to increased concentrations of Pb in ecosystems (Pepi et al., 2016). Excessive Pb can be discharged into aquatic systems through atmospheric deposition, wastewater discharge, stormwater runoff and flood deposit and become hazardous to aquatic organisms and humans (Zohar et al., 2014).

Sediments both take and release Pb from the water column. Typically, Pb is initially adsorbed by the suspended particles in water, due to a series of processes, such as co-precipitation, hydrolysis, and deposition into the sediment (Niu et al., 2015). The concentrations of dissolved Pb in the water column are typically orders of magnitude lower than those in sediments (Patel et al., 2018). After sediment deposition, Pb can be released into the overlying waters due to changes of chemical and biological conditions in the sediment (Hill et al., 2013). Since Fe/Mn oxides have been reported to be a major binding phase for Pb in sediments (Kushwaha et al., 2018), the acidic and anaerobic conditions could increase the rates of reduction and dissolution of oxides of iron (Fe) and manganese (Mn) (Chakraborty et al., 2016), leading to the liberation of Pb into the water. The increase of dissolved organic matter (DOM) also has the potential to increase Pb solubility under neutral pH conditions by the generation of complexes (Sauve et al., 1998). Contrarily, formation of stable Pb phases such as Pb-sulfide under anaerobic conditions and Pb-phosphate minerals can alleviate Pb release (Cai et al., 2017; Wolfe and Wilkin, 2017).

Lake eutrophication and harmful algal blooms (HABs) have become global environmental problems. Lake eutrophication often results in the imbalance of ecosystems, causing harm to aquatic and terrestrial wildlife and human health (Del Giudice et al., 2018). Total Pb content in sediments has been reported to be greatly increased by HABs (Baptista et al., 2014; Garcia-Hernandez et al., 2005). For example, it was observed that the total Pb contents in sediments were 3 times higher than the background concentrations during the dinoflagellate blooms (Garcia-Hernandez et al. (2005)). Also, a similar phenomenon was found, suggesting that total Pb contents in sediments were significantly increased to potentially toxic levels due to cyanobacterial blooms (Baptista et al., 2014). The authors inferred that *Microcystis aeruginosa* adsorbed Pb and deposited it in the sediments rapidly, leading to increased concentrations of Pb in the sediments. However, up to date, the effects of water eutrophication and algal blooms on Pb mobility, rather than total Pb contents, in sediments have rarely been studied. The physiological activity of live algae and the decomposition of dead algae can significantly change the chemical and biological environments in the water column and sediments (Han et al., 2015), likely leading to profound seasonal variation of Pb mobility in the sediment-water systems. There is a lack of field evidence for this assumption, and a comprehensive understanding of Pb mobility and possibly induced Pb pollution is worthy of further study.

The changes of mobile Pb (e.g. dissolved Pb in pore water and easily exchangeable Pb in sediment solids) can directly contribute to the variations of Pb concentrations in the water column (Banks et al., 2012). Accordingly, understanding the changes in mobile Pb in sediments is very useful for evaluating Pb contamination and toxicity in aquatic systems. However, previous Pb assessments were often based on changes in total mass of Pb. This method is not effective enough to characterize Pb mobility in sediments, because a part of Pb in sediments is inert (Wang et al., 2016a). The chemical extraction methods are also often used, but they have poor precision and selectivity due to operational inconsistency and species redistribution (Wang and Mulligan, 2008). On the other hand, sediments demonstrate significant heterogeneity in biogeochemical properties along the vertical direction (Ding et al., 2015; Santner et al., 2015), while this aspect has been rarely studied due to the difficulty in sampling. This challenge has been overcome by the recently developed techniques like high resolution dialysis (HR-Peeper) and diffusive gradients in thin films (DGT). These two kinds of passive sampling techniques can measure dissolved Pb in pore water and labile Pb in sediments at a mm-scale vertical resolution, respectively (Wang et al., 2017; Xu et al., 2012).

Our purpose was to study the variations of the Pb mobility in the sediments of a eutrophic body of water over a full year and explore the mechanisms behind. A hyper-eutrophic bay was selected and monthly sampling was performed to obtain the vertical distributions of the dissolved and labile Pb using HR-Peeper and DGT, respectively. To elucidate the underlying mechanisms of Pb mobilization, two microcosm experiments were realized to elucidate the temporal influence on Pb mobility of algal bloom and redox conditions using an intensive sampling frequency.

2. Materials and methods

2.1. Location of study

Lake Taihu is the third largest freshwater lake in China. Due to the fast escalation in urban and agricultural generation of nutrients, Lake Taihu has become highly eutrophic and presents toxin-producing, increasingly intense cyanobacterial blooms (Xu et al., 2017). Meiliang Bay is located in the northern Lake Taihu, which is one of the most eutrophic regions of the lake (Yang et al., 2016).

The sampling site was in Meiliang Bay near the Taihu Laboratory for Lake Ecosystem Research (TLLER) (31°26′18″N, 120°11′12″E), Nanjing Institute of Geography and Limnology (Fig. 1). The basic water and sediment quality characteristics in this location have been studied previously and are listed in Tables S1 and S2 (Ding et al., 2018; Jin et al., 2019). During the sampling periods between February 2016 to January 2017, the Chl-*a* and DO concentrations of the water column in the sampling site varied from 12.3 to 178.4 μg/L and from 5.95 to 12.2 mg/L, respectively. The water column had dissolved organic carbon (DOC) concentrations in the water column ranged from 2.60 to 6.88 mg/L, with the highest value found in July. The oxygen penetration depth (OPD) in sediments varied from 0.6 to 3.6 mm, with the high and low values in winter and summer months, respectively. The bacterial abundance varied from 1.33E+11 to 11.4E+11 copies/g, with the highest value in March.

The monthly changes in the distributions of dissolved Fe/Mn and DGT-labile Fe/Mn have been determined previously in the sampling site (Ding et al., 2018; Jin et al., 2019). Their mean concentrations in the top 5 cm sediment layer are shown in Table S2. The highest values for the concentrations of dissolved Mn were found in March for dissolved Mn, and in February for DGT-labile Mn. The highest DGT-labile Fe concentrations were observed in June and July, while the lowest concentrations were observed in December and January.

2.2. Preparation of the HR-Peeper and DGT probes

The devices were provided by EasySensor Ltd. (www.easysensor.net). The Supplementary material includes a detailed description of the operating principles. The HR-Peeper device had a resolution of 4.0 mm and was used for the measurement of dissolved Pb in sediment pore water (Ding et al., 2018). At first, the devices were filled with deionized water and covered by a Durapore® PVDF membrane (Millipore, 0.45 μm pore size, 0.10 mm thickness). The ZrO-Chelex DGT was used for the measurement of labile Pb in sediments (Wang et al., 2017). First, the ZrO-Chelex DGT probe, the binding gel was covered by an agarose diffusive gel and then a Durapore® PVDF membrane (Wang et al., 2017). The AgI DGT devices were used for the measurement of labile sulfide(-II) in sediments, as in Ding et al. (2012). The probes were immersed in 0.01 M NaCl solutions and then deoxygenated with a nitrogen flow for at least 16 h, before their utilization.

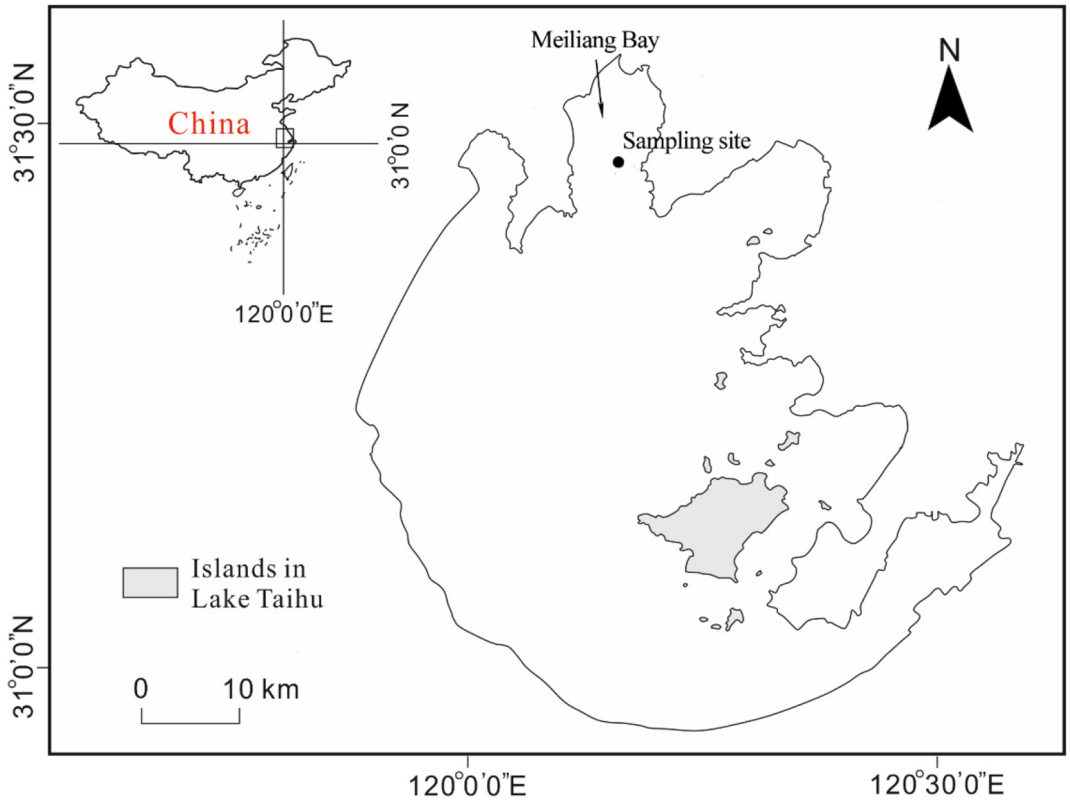

Fig. 1. Study area in Meiliang Bay, Lake Taihu (modified from Chen et al., 2018).

2.3. Field investigation

Water samples and six replicate sediment cores (with 4 more cores in January, April, July and October) were collected to measure Pb in solution and DGT-labile Pb monthly, and labile S(-II) seasonally between February 2016 and January 2017, with a gravity corer (dia. 11 cm). The sampling time was in the middle of each month (around the 15th). The water samples and sediment cores were taken and moved to the lab in 3 h or less, with the water at a depth of 20 cm. Sections of 1 cm down to a depth of 10 cm were taken from three cores under the N_2 gas and the samples of 0–10, 30–40 and 90–100 mm sediment layers were frozen-dried and used for Pb species analysis by a modified extraction method (BCR) (Nemati et al., 2011). This method has three steps and separates the Pb components into four fractions: acid extractable/exchangeable fraction (F1), easily reducible fraction (F2), oxidizable fraction (F3) and residual fraction (F4).

Three cores were kept overnight at the same temperature as the field using a water bath. Then, a HR-Peeper probe was introduced into each core, and the DGT probes were then introduced 24 h later, and the probes were left for another 24 h. At that moment, all were retrieved simultaneously. After retrieval, the HR-Peeper, AgI DGT and ZrO-Chelex DGT probes were treated as described in Ding et al. (2018), Ding et al. (2012) and Wang et al. (2017) respectively. Immediately, the device surface was briefly washed with deionized water. Then the pore and overlying water in the HR-Peeper devices were promptly transferred to 0.5 mL centrifuge tubes for analysis. The ZrO-Chelex binding gels were sliced, and the labile Pb in the binding gel is then eluted with a 1.0 HNO_3 solution.

Four sediment cores in January, April, June, and October were divided in sections of 1 cm down to a depth of 5 cm under N_2 gas. The sediment was centrifuged at 4000 rpm (1900g) for 10 min and the water collected by filtration with a Whatman 0.45 μm cellulose nitrate membrane. The top 5 mm sediments were frozen-dried and used for analysis of acid volatile sulfide (AVS) and pyrite using the methods reported by Yin et al. (2008).

2.4. Cyanobacterial bloom experiment

The details of the cyanobacterial bloom experiment were explained in Chen et al. (2018). Water, algae and three sediment cores (dia. 11 cm,

Table 1
Concentrations of dissolved Pb in overlying water and comparison with different national and international guidelines (the ratio to the criterion value >1 is highlighted in bold).

Month	Dissolved Pb (μg/L)	Ratio to the criterion value			
		Dissolved Pb/CNEQS 1[a]	Dissolved Pb/CNEQS 2[b]	Dissolved Pb/WHO[c]	Dissolved Pb/EPA-CMC[d]
2016-2	20.79	**2.08**	0.42	**2.08**	0.32
2016-3	23.33	**2.33**	0.47	**2.33**	0.36
2016-4	34.75	**3.48**	0.70	**3.48**	0.53
2016-5	49.06	**4.91**	0.98	**4.91**	0.75
2016-6	50.09	**5.01**	**1.00**	**5.01**	0.77
2016-7	118.5	**11.85**	**2.37**	**11.85**	**1.82**
2016-8	78.85	**7.89**	**1.58**	**7.89**	**1.21**
2016-9	46.65	**4.67**	0.93	**4.67**	0.72
2016-10	75.78	**7.58**	**1.52**	**7.58**	**1.17**
2016-11	79.08	**7.91**	**1.58**	**7.91**	**1.22**
2016-12	46.83	**4.68**	0.94	**4.68**	0.72
2017-1	44.81	**4.48**	0.90	**4.48**	0.69
Criterion Limit (μg/L)		CNEQS 1[a] 10	CNEQS 2[b] 50	WHO[c] 10	EPA-CMC[d] 65

[a] Standard for drinking water quality in China (GB 5749-2006).
[b] Standard for fisheries water quality in China (GB 11607–89).
[c] Drinking water standard of World Health Organization (WHO).
[d] Criteria maximum concentration (CMC) for Pb in freshwater set by Environmental Protection agency.

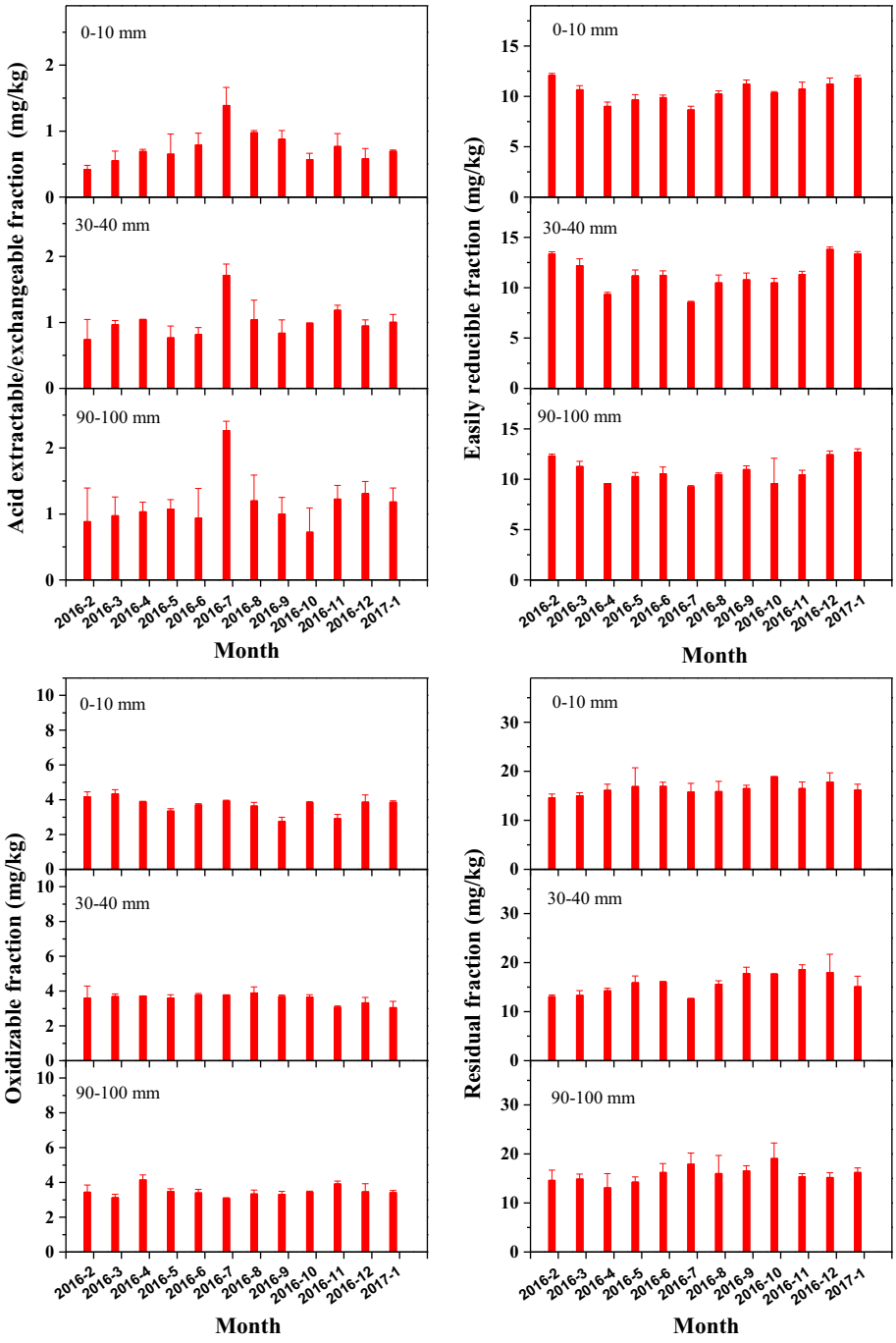

Fig. 2. Lead fractionation in Meiliang Bay sediments (Data in April, July, October 2016 and January 2017 are cited from Chen et al., 2019).

l. 30 cm) were collected. Five Rhizon samplers (Rhizon CSS, the Netherlands, dia. 2.5 mm) were installed in the sediment cores. They were inserted horizontally in the overlying water at 5 mm above the sediment-water interface (SWI) and below at depths of −5 mm, −10 mm, −15 mm and −20 mm. Then the three sediment cores were placed in a container and left for 2 days in a glasshouse. Then, 10 L of unfiltered lake water containing algae was added to the container. The containers were continuously kept in the glasshouse for 70 days. Evaporation caused a loss of water, so filtered lake water was added to the container every 2–3 days. Samples of approximately 1 mL volume of overlying and pore waters from different sediment depths were obtained via Rhizon samplers before (Day 1) and after algae addition (Days 5, 15, 44 and 70) every 3 h (at 9:00, 12:00, 15:00, 18:00, 21:00, 0:00, 3:00, 6:00) for the analysis of dissolved Pb. According to Chen et al. (2018), Day 5, Day 15 and Day 44 represented the algae growth period, the peak period of algal blooms and bloom collapse period, respectively, reflected by changes of Chl-*a* concentrations on each sampling day.

2.5. Aerobic-anaerobic experiment

Sediment samples with water were collected with three cores (dia. 11 cm, l. 30 cm). Each sediment core had three Rhizon samplers installed below the SWI at depths of −5 mm, −15 mm and −50 mm,

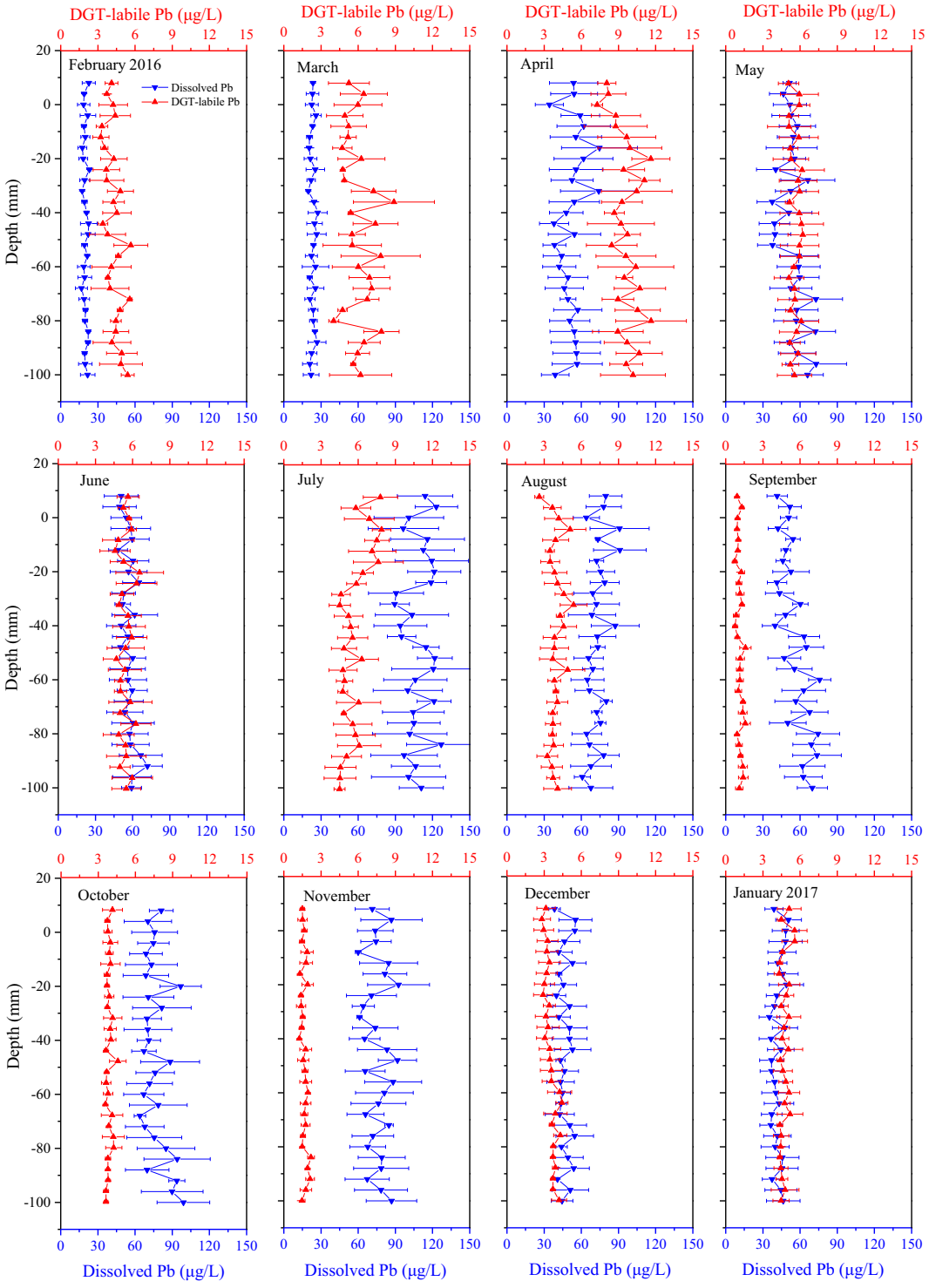

Fig. 3. Vertical distributions of dissolved Pb and DGT-labile Pb in the overlying water-sediment profiles of Meiliang Bay from February 2016 to January 2017 (Data of dissolved Pb and DGT-labile Pb in April, July, October 2016 and January 2017 are cited from Chen et al., 2019).

respectively. The cores were installed in a container, covered with filtered lake water (Whatman, 0.45 mm pore size), and kept at 25 °C with a water bath. The experiment was first incubated as control without treatment for 24 h; then an aerobic incubation (pumping O_2) (0.4 L/min) for 176 h; then an anaerobic incubation (pumping N_2) (0.4 L/min) for 376 h. Samples of approximately 1 mL of overlying and pore waters in different sediment depths were obtained via Rhizon samplers in the control, aerobic and anaerobic treatments every 4 h for analyzing dissolved Pb, Fe and Mn, and DOM.

2.6. Sample analysis

The samples from the HR-Peeper, ZrO-Chelex DGT, and pore waters, were analyzed for Mn and Pb with a ICP-MS spectrometer (Agilent Technologies 7700×, USA) after dilution using 3% HNO_3. The concentrations of Fe were determined by the phenanthroline colorimetric method (Tamura et al., 1974). DGT-labile S(-II) in sediments was measured through the analysis of a computer-imaging densitometry (CID) technique (Ding et al., 2012). Free ionic Pb in pore water was analyzed

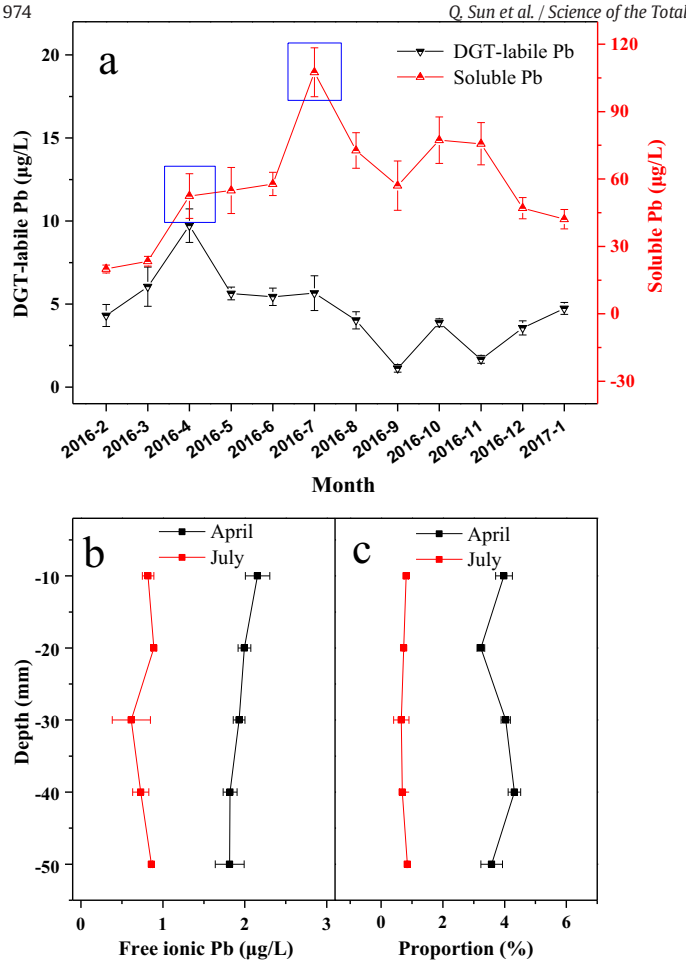

Fig. 4. Monthly changes of mobile Pb and dissolved Pb speciation in Meiliang Bay sediments. (a) Monthly changes of dissolved Pb and DGT-labile Pb concentrations in sediment profiles (0 mm to −100 mm vertically averaged) between February 2016 and January 2017. (b) Vertical distribution of free ionic Pb concentrations in sediment pore waters in April and July, and (c) proportions of free ionic Pb relative to dissolved Pb in sediment pore waters in April and July.

using a multifunctional portable heavy metal analyzer using voltammetric technique (the limit of detection is 0.5 μg/L; HM-5000P, Skyray, China) (Lu, 1999). The concentrations of DOC were evaluated by the UV254 absorbance using Epoch Microplate Spectrophotometer (BioTek, USA) or using a Shimadzu TOC-L analyzer equipped with an ASI-L auto-sampler (Tue-Ngeun et al., 2005).

2.7. Data processing

The flux of DGT-labile S(-II), and the concentrations of DGT-labile Pb in the sediment-water profile were calculated as Eqs. (1) and (2) (Li et al., 2019):

$$F_{DGT} = M/At \quad (1)$$

$$C_{DGT} = M\Delta g/DAt \quad (2)$$

where M represents the accumulated mass over the deployment time; A represents the gel exposure area (30 cm^2); t represents the deployment time (24 h); Δg represents the diffusive layer thickness (0.90 mm); D is the diffusion coefficient of Pb in the diffusive layer (8.41×10^{-6} cm^2/s at 25 °C) (Wang et al., 2016b).

Statistical analyses were performed using SPSS v19.0 software. One-way ANOVA method was used to analyze the significant differences in dissolved Pb between different experiments. The correlations between each two variables were analyzed using the Pearson correlation coefficient.

3. Results

3.1. Field investigation

The concentrations of dissolved Pb in the water over the sediments of Meiliang Bay are displayed in Table 1. The values ranged from 20.79 to 118.5 μg/L, with the maximum value in July. The Pb speciation from chemical fractionation in the sediments is shown in Fig. 2. Pb contents ranged from 0.42 to 2.27 mg/kg for acid extractable/exchangeable fraction, 8.68 to 13.83 mg/kg for easily reducible fraction, 2.76 to 4.68 mg/kg for oxidizable fraction, and 12.65 to 19.08 mg/kg for residual fraction. For the acid extractable/exchangeable fraction, the highest contents were observed in July in sediment layers of 0–10 mm (1.39 mg/kg), 30–40 mm (1.71 mg/kg) and 90–100 mm (2.27 mg/kg), while the lowest Pb contents were observed in February (0.42 mg/kg) and March (0.55 mg/kg) in 0–10 mm sediment layers. For the easily reducible fraction, Pb contents were consistently lower in July and April than the other months in different sediment layers. The contents of AVS and pyrite in sediments are shown in Fig. S1. The contents were below 27 mg/kg (AVS) and 136 mg/kg (pyrite) in January and April, and the values increased to 42 mg/kg (AVS) and 266 mg/kg (pyrite) in July and October.

Fig. 3 shows the distributions of Pb dissolved in pore waters and DGT-labile Pb. The concentrations of both types of Pb displayed small fluctuations in the vertical profile without obvious trends. Average concentrations of both types in the vertical profiles are shown in Fig. 4a. In the winter months (December, January and February), the mobile Pb concentrations were low and stable, followed by increases in March and April. For the summer months, dissolved Pb was at the highest concentration in July (107.5 μg/L), while DGT-labile Pb was relatively low and stable in the summer months (4.02–5.66 μg/L). For the autumn months, the concentrations of both types decreased in September and then increased in October. The concentrations of free ionic Pb in pore waters ranged from 1.82 to 2.16 μg/L in April and from 0.62 to 0.87 μg/L in July in sediment profiles (Fig. 4b). The proportion of free ionic Pb relative to dissolved Pb ranged from 3.32% to 4.18% in April and from 0.48% to 0.86% in July (Fig. 4c).

The distributions of DGT-labile S(-II), both one and two-dimensional, during March, July, September and December are shown in Fig. 5. A great variation was observed in the level of DGT-labile S(-II) among the four months. The highest level appeared in July and then September, which was up to 102 times higher than the lowest observed in December.

3.2. Cyanobacterial bloom experiment

In the cyanobacterial bloom experiment, the hourly changes and mean values of dissolved Pb concentrations in the overlying water-sediment profiles on days 1, 5, 15, 44 and 70 after algae addition are shown in Figs. 6 and 7, respectively. Before algae addition (Day 1), the mean concentrations of dissolved Pb in overlying water-sediment profiles ranged from 14.45 to 23.40 μg/L (Fig. 7), and the dissolved Pb concentrations obviously fluctuated at different sampling hours (Fig. 6). After addition of algae on Day 5 and Day 15, the concentrations of dissolved Pb in overlying water-sediment profiles decreased by 29.0–55.8% and 40.0–59.1%, respectively (Fig. 7), and the dissolved Pb became more stable at different sampling hours (Fig. 6). On Day 44, the dissolved Pb significantly increased ($p < 0.05$) in overlying water and at most of the sediment depths by 26.1–191% compared to Day 1 (Fig. 7). On Day 70, the dissolved Pb concentrations decreased by 29.2–86.9% in overlying water-sediment profiles.

3.3. Incubation experiment under aerobic-anaerobic conditions

The hourly variations in the concentrations of dissolved Pb, Fe and Mn are shown in Fig. 8a. In both the control and aerobic incubations, the concentrations of dissolved Pb remained relatively stable in the range of 9.01–20.78 μg/L. The concentrations of dissolved Pb increased under anaerobic incubation compared to the control, and the mean concentrations ranged from 36.00 to 38.39 μg/L (Fig. 8a) in overlying water-sediment profiles. The dissolved Fe and Mn decreased in the sediments in aerobic incubation (Fig. 8a). In the anaerobic incubation, dissolved Fe and Mn concentrations showed 2.4- and 2.3-fold increases on average, respectively, comparing to those in aerobic incubation (Fig. 8a). A simultaneous increase of dissolved Mn and Pb appeared at the beginning of the anaerobic incubation (344–352 h), implying that the release of Pb was partly attributed to the reduction of Mn oxides.

The hourly variations of UV254 absorbance are shown in Fig. 8b. UV254 absorbance in sediment profiles remained relatively stable in control and aerobic incubations, while it slightly decreased at the beginning of the anaerobic treatment (344–420 h), sharply increased after 423 h and sharply decreased after 496 h (Fig. 8b). Simultaneous increases and decreases for dissolved Pb and UV254 absorbance were observed at 344–420 h. They both increased at 359 h, 376 h, 388 h and 420 h, and decreased at 344 h, 348 h, 372 h and 404 h in sediment profiles. It provided a strong evidence for the formation of DOM-Pb complexes at 344–420 h.

4. Discussion

4.1. Comprehensive evaluation of Pb contamination

Previous studies have investigated Pb contamination and the associated ecological risks in Lake Taihu by assessing the total concentrations of Pb in the water, sediment and aquatic organisms (Fu et al., 2013; Niu et al., 2015). Fu et al. (2013) found that the total Pb concentrations were much greater in the sediments of Yangtze River than those in the sediments of Lake Taihu, while lower in the fish from Yangtze River than in the fish from Lake Taihu. Niu et al. (2015) found that Pb concentrations in the sediments of Lake Taihu increased and their mean concentrations were far greater than the basin background values. The north bays (including Meiliang Bay) had higher total Pb concentrations than the remaining parts of Lake Taihu. These results likely indicated a persistent Pb pollution in the sediments of Lake Taihu, especially in the northern part, due to the discharge of domestic sewage and industrial wastewater (Yin et al., 2011).

Different national and international guidelines for Pb concentration in water are shown in (Table 1). A comparison of the values of the dissolved Pb concentrations found in this study with those in Table 1 confirms the high Pb pollution in this area. In this work, dissolved Pb concentrations in the overlying water of Meiliang Bay (20.79–118.5 μg/L) showed values higher than those of the drinking water standards in China and of the World Health Organization (10 μg/L) for all the 12 months. The values also exceeded the limit value of fisheries water quality standard (50 μg/L) in China set by Administration of Environmental Protection of China in June, July, August, October and November 2016, and the criteria for maximum concentration (CMC) for Pb in freshwater (65 μg/L) set by the U.S. Environmental Protection Agency (US EPA) in July, August, October and December 2016. The changes of overlying water dissolved Pb is consistent with the report by Rajeshkumar et al. (2018) in Lake Taihu, in which the total Pb concentrations in water samples as well as the accumulation of Pb in sediments, fishes and oysters were higher in the summer than in the spring.

4.2. Pb mobility in sediments and the underlying mechanisms

The concentrations of mobile Pb in sediments exhibited notably seasonal variation (Fig. 4a). In the months of winter (7.5 °C ≤ T ≤ 10.5 °C, 10.05 mg/L ≤ DO ≤12.21 mg/L, Table S1), the mobile Pb concentrations were low and stable, followed by increases in March (T = 10.5 °C, DO = 10.05 mg/L, Table S1) and April (T = 20.0 °C, DO = 10.02 mg/L, Table S1). For the summer months (26.1 °C ≤ T ≤ 31.2 °C, 5.95 mg/L ≤ DO ≤8.21 mg/L, Table S1), dissolved Pb was at the highest concentration in July (107.5 μg/L), while DGT-labile Pb was relatively low and

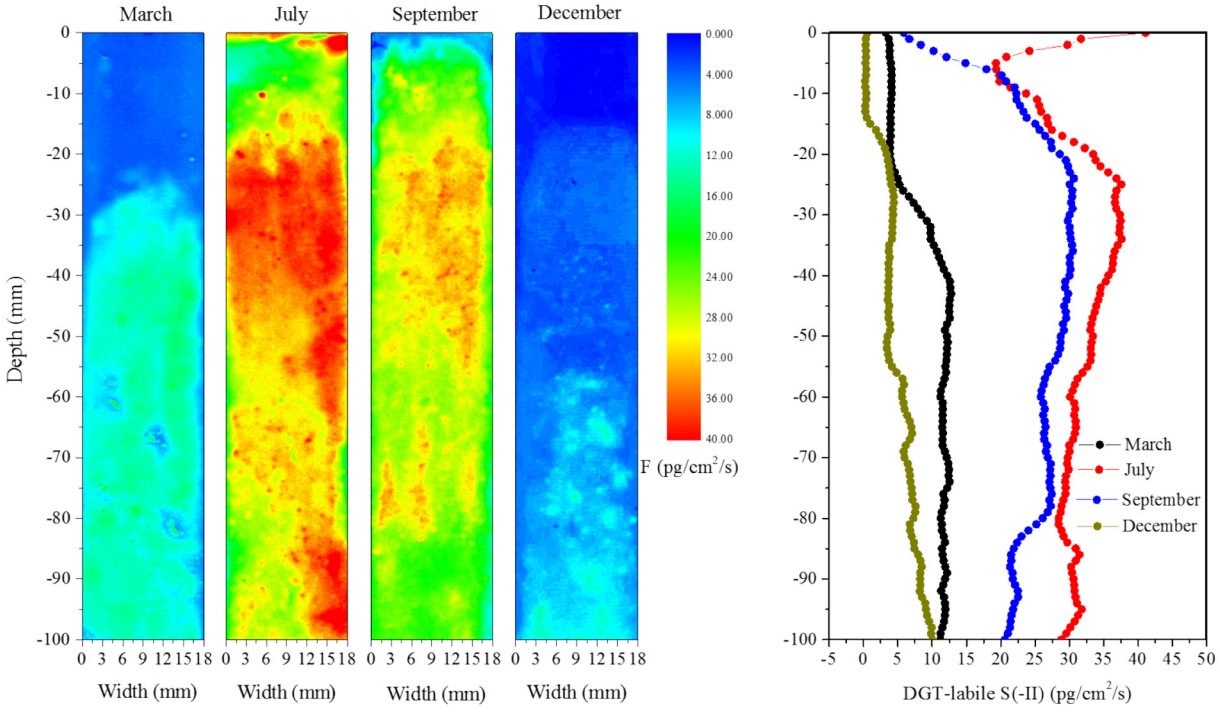

Fig. 5. Seasonal changes of 2D DGT-labile S(-II) flux (left) and horizontal average (right) in March, July, September and December 2016.

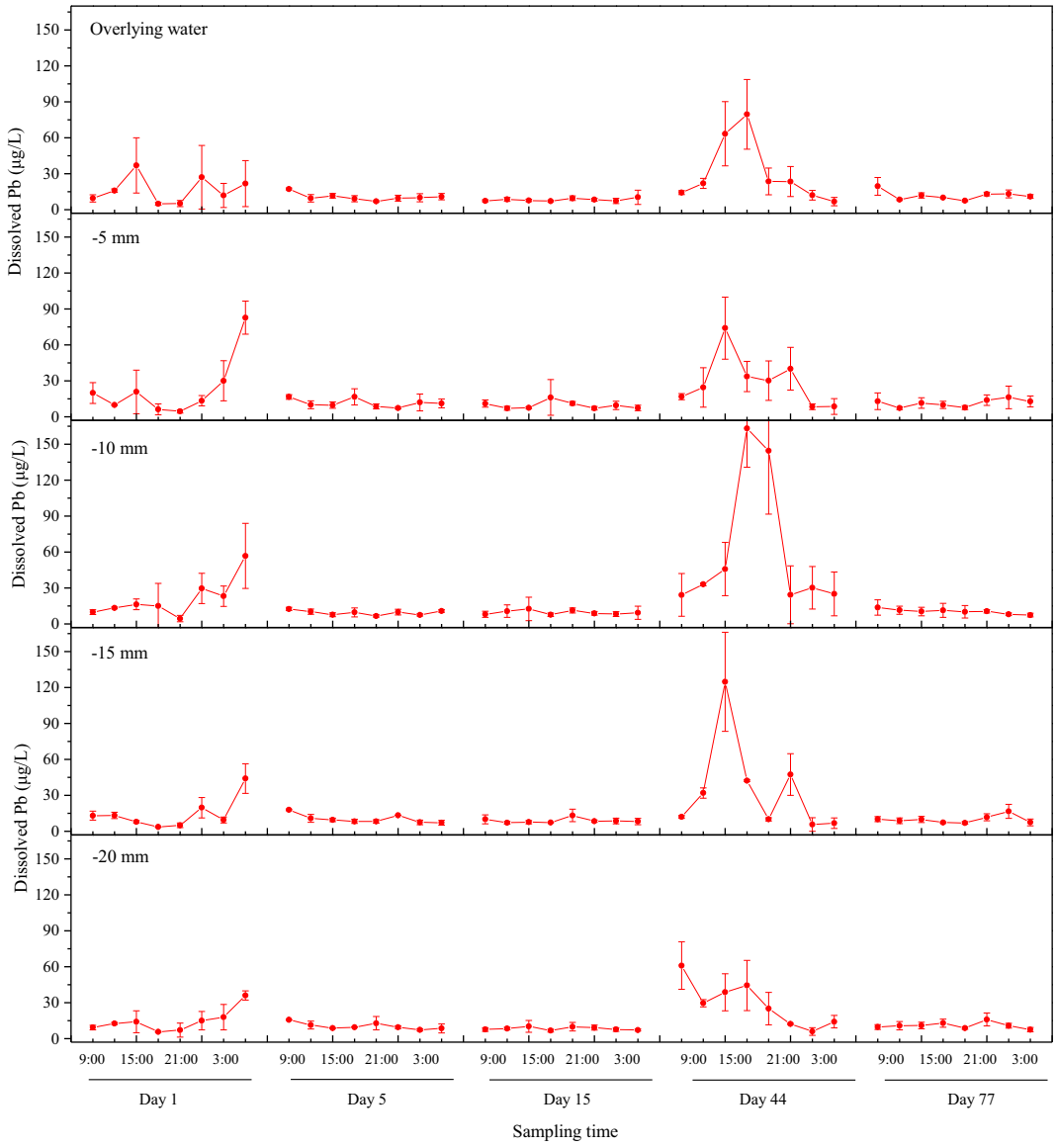

Fig. 6. Hourly changes in dissolved Pb concentrations in overlying water and sediment depths of −5 mm, −10 mm, −15 mm and −20 mm on Day 1, 5, 15, 44 and 70, respectively.

stable in the summer months (4.02–5.66 μg/L). For the autumn months (16.1 °C ≤ T ≤ 24.8 °C, 7.21 mg/L ≤ DO ≤9.67 mg/L, Table S1), the concentrations of both Pb types declined in September and then rose in October.

Since there was a consistent distribution of dissolved Pb between the overlying water and the sediment (Figs. 3–4), the pollution of Pb in overlying water should be caused by the mobilization of Pb from sediments. Thus, it becomes necessary to explore the underlying mechanism for Pb mobility in sediments. The mechanisms controlling the seasonal mobilization of Pb are discussed as follows, according to the monthly variations of dissolved and DGT-labile Pb in sediments.

4.2.1. Winter and early spring (December to April)

Meiliang Bay sediments were under a consistently oxidizing condition, characterized by high DO (10.05–12.21 mg/L) in water column, and high Eh (322.6–394.3 mV) and high oxygen penetration depth (OPD) values (2.6–3.6 mm) in sediments (Tables S1 and S2). In winter, most Fe was in oxidized forms, reflected by the low concentration of dissolved Fe in surface sediments (0.29–0.46 mg/L, Table S2). Also, the formation of DOM-Pb complexes relative to other months was not favored in winter due to the low concentrations of DOC in the overlaying water (2.60–3.26 mg/L). Dissolved and DGT-labile Pb was low (Figs. 3–4) and stable which should be primarily immobilized by Fe/Mn oxides in winter, since these oxides are a major binding phase for Pb in sediments (Kushwaha et al., 2018). This is verified by the relatively high contents of reducible fraction of Pb (mainly Fe/Mn oxides binding Pb) in sediments in winter compared to other seasons (Fig. 2).

Sharp increases in dissolved and DGT-labile Pb were observed from March to April (Fig. 4a). The highest bacterial abundance was observed in March, in comparison with previous months (Table S2). Furthermore, high concentrations of dissolved Mn (2.77 mg/L) in March and dissolved Fe (2.37 mg/L) in April was observed in sediments (Table S2). The increases in bacterial abundance in the sediment, which is a response for temperature rise, likely favored the reduction of Fe/Mn oxides (Ding et al., 2018). The immobilized Pb by Fe/Mn oxides in winter could be easily released under reducing conditions (Tack et al., 2006), resulting in the increased concentrations of dissolved and DGT-labile Pb (Fig. 4a). This inference was consistent with the decrease in content of reducible fraction of Pb (F2) in April compared to those in winter (Fig. 2). It was also supported by the simultaneous releases of Pb and

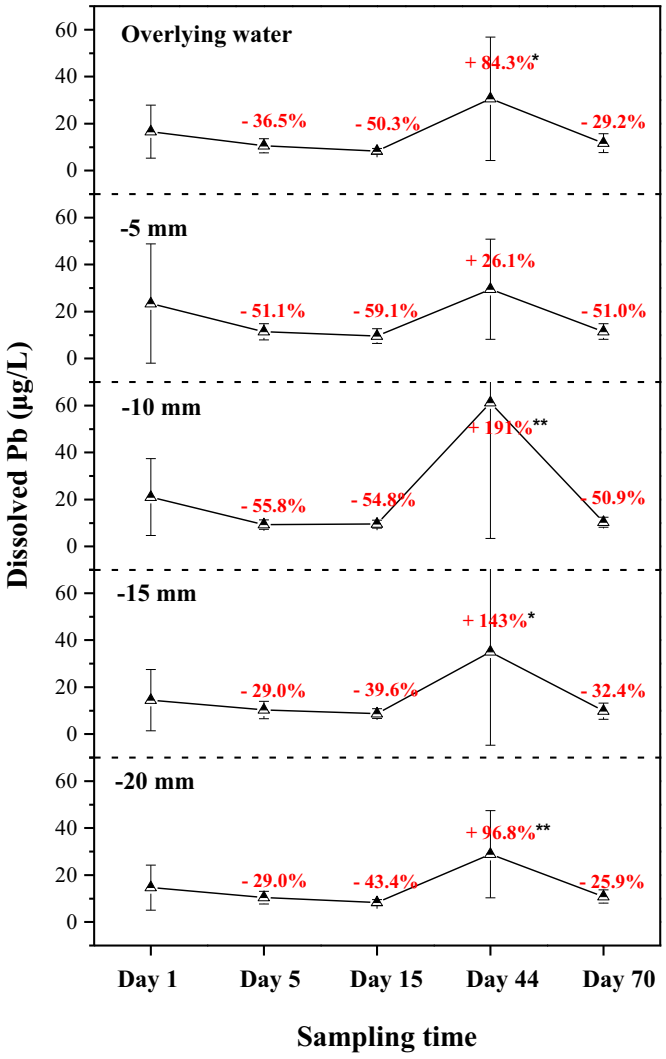

Fig. 7. Mean concentrations of dissolved Pb in overlying water-sediment profiles on Day 1, 5, 15, 44 and 70 in cyanobacterial bloom experiment. The red values above the symbols represent the percentage of increase or decrease relative to the values on Day 1. *, ** indicate that difference is significant at 0.05 and 0.01 levels, respectively.

Mn at the beginning of the anaerobic incubation in the aerobic-anaerobic experiment (Fig. 8a).

4.2.2. Summer (June to August)

The dissolved Pb concentrations of dissolved Pb in Meiliang Bay peaked in July, while DGT-labile Pb concentrations were relatively low and stable across the summer (Fig. 4a). Chl-*a* concentrations in water of Meilaing Bay drastically increased from 64.3 μg/L in June to 153.4 μg/L in August, indicating a severe outbreak of algal blooms during this season (Table S1). Algal blooms can create reducing conditions by obstructing the transfer of oxygen from air to water and consuming oxygen during decomposition of dead algae (Wang et al., 2015). The reducing extent became stronger from April to July, reflected by the decrease in the penetration depth of oxygen from 3.0 to 1.0 mm (Table S2). Hence, the reduction of Fe/Mn oxides (especially Fe oxides; Table S2) should be promoted especially after the algal blooms in June, resulting in a sharp release of dissolved Pb from June to July (Fig. 4a). Higher Pb content in acid extractable/exchangeable fraction and lower Pb content in reducible fraction were observed in July, indicating that the released Pb should be transformed into more labile phase (Fig. 2).

On the other hand, Pb ion can be easily redistributed through the adsorption and precipitation processes in sediments (Howard and Vandenbrink, 1999), but these immobilization processes could be inhibited by DOM-Pb complexes formed in solution (Hashimoto et al., 2009a). In this study, the anaerobic mineralization of both endogenous organic matter (Yao et al., 2011) and labile organic matter from dead algae (Leao et al., 2007) provided abundant organic ligands in July (DOC = 6.88 mg/L, Table S1), creating favorable conditions for the formation of DOM-Pb complexes. Accordingly, the free Pb ion measurement showed greater proportion of Pb complexes in pore water in July in comparison with that in January and April (Fig. 4b, c). Because metal-DOM complexes cannot be directly taken up by DGT (Wang et al., 2018), the DGT-labile Pb concentrations were found to be relatively stable at a low level in summer (Fig. 4a). This hypothesis was supported by the formation of DOM-Pb complexes between 344 and 420 h under anaerobic incubation (Fig. 8b). It implied that the complexation of Pb by DOM played a dominant role in stabilizing mobile Pb in pore water following the release of Pb from reduction of Fe/Mn oxides, which further enhanced the mobility of Pb in summer.

4.2.3. Autumn (September to November)

Peak concentrations were observed for dissolved Pb (77.27 μg/L) and DGT-labile Pb (3.88 μg/L) in October (Fig. 4a), which were much lower than those observed in July. Before this peak in October, the concentrations of dissolved and DGT-labile Pb exhibited sharp decreases from July to September. The accumulation of high amounts of Pb by cyanobacteria has been shown (Kumar et al., 2015; Rzymski et al., 2014). The Pb ion can be adsorbed or assimilated by live or dead algae (Chakraborty et al., 2011; Kumar et al., 2015; Kushwaha et al., 2018) and then deposited onto sediments. Since the concentration of Chl-*a* was the greatest in August (Table S1), the decreases in concentrations of dissolved Pb and DGT-labile Pb after July were attributed to bioaccumulation of Pb by live algae cells and adsorption of Pb to dead algae cells.

In September and October, the concentrations of Chl-*a* in water column of Meiliang Bay decreased (38.9 and 53.4 μg/L, respectively; Table S1). The bacterial diversity in sediments was higher in October (6.25E+11 copies/g; Table S2), indicating that there was an intense bloom collapse especially in October. The breakdown of the cyanobacterial blooms, caused the liberation of complex substances that are not easily processed by microorganisms, as well as biodegradable and labile molecules (Han et al., 2015; Lezcano et al., 2017). Pb previously immobilized by algae can thus be released again during the decomposition of algal residues, leading to the increase of mobile Pb in overlying water-sediment profiles in October (Fig. 4a). Results of the cyanobacterial bloom experiment further proved that Pb was immobilized in August and September by algal bioaccumulation and released in October due to algal decomposition (Figs. 6–7). However, the release of Pb in October in the field was less pronounced than observed on Day 44 in the microcosm experiment. The limited height of the overlying water and the high density of algae in the microcosm experiment should account for the discrepancy between natural and microcosm incubations.

On the other hand, the contents of AVS and pyrite in sediments obviously increased from April to June and maintained at high levels until October. Their increases resulted from a high level of labile sulfide in sediments in the summer and autumn detected by DGT (Fig. 5). It has been revealed that the enhanced sulfide was produced from sulfate reduction during algal decomposition (Garcia-Hernandez et al., 2005). The released Pb from reduction of Fe/Mn oxides should be further immobilized through the precipitations of Pb-sulfides (PbS, $Ksp = 8.0 \times 10^{-28}$), which are thermodynamically stable and in less bioavailable phases (DeVolder et al., 2003; Hashimoto et al., 2009b). In addition, it has been reported that pyrite is a suitable adsorbent for Pb^{2+} (Ozverdi and Erdem, 2006), and this adsorbent has been used for removal of Pb^{2+} in wastewater (Yang et al., 2017). The pyrite adsorption, in combination with sulfide precipitation, should significantly suppressed the

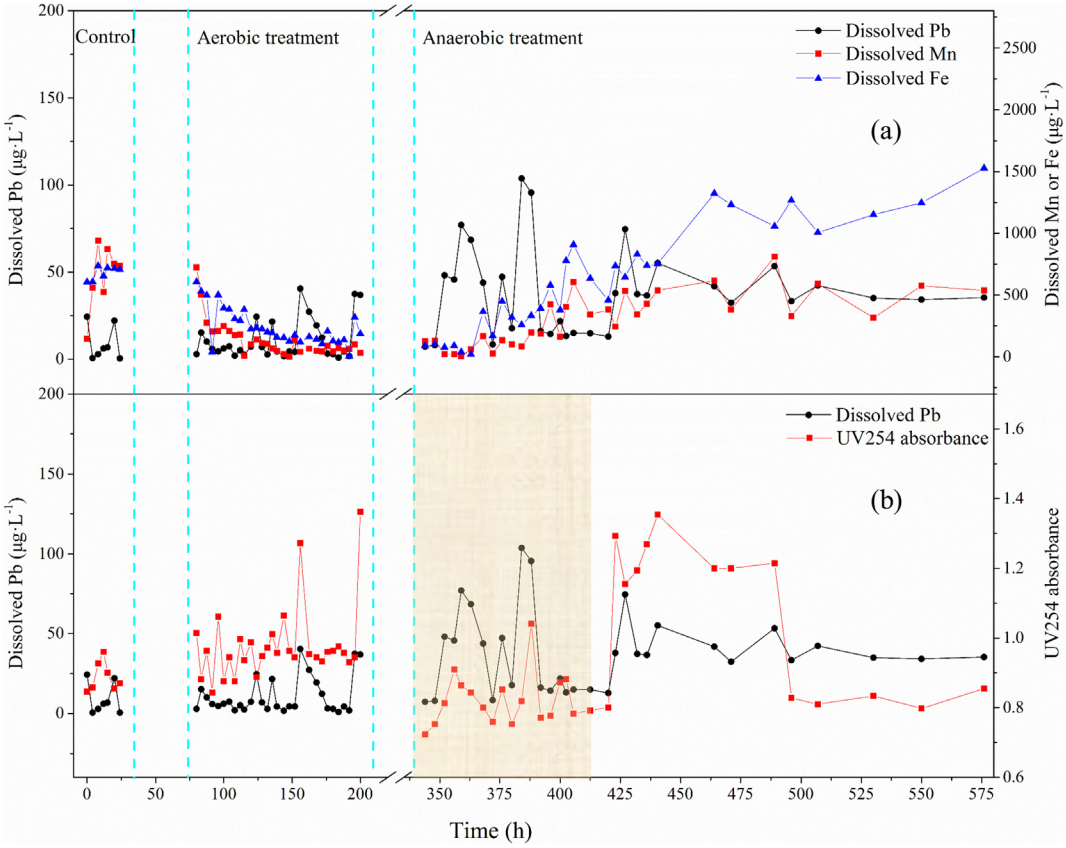

Fig. 8. Hourly changes in (a) dissolved Pb, Fe and Mn, and (b) dissolved Pb and UV254 absorbance in sediment pore waters in aerobic-anaerobic experiment. The part with the fill pattern in (b) shows simultaneous changes for dissolved Pb and UV254 absorbance.

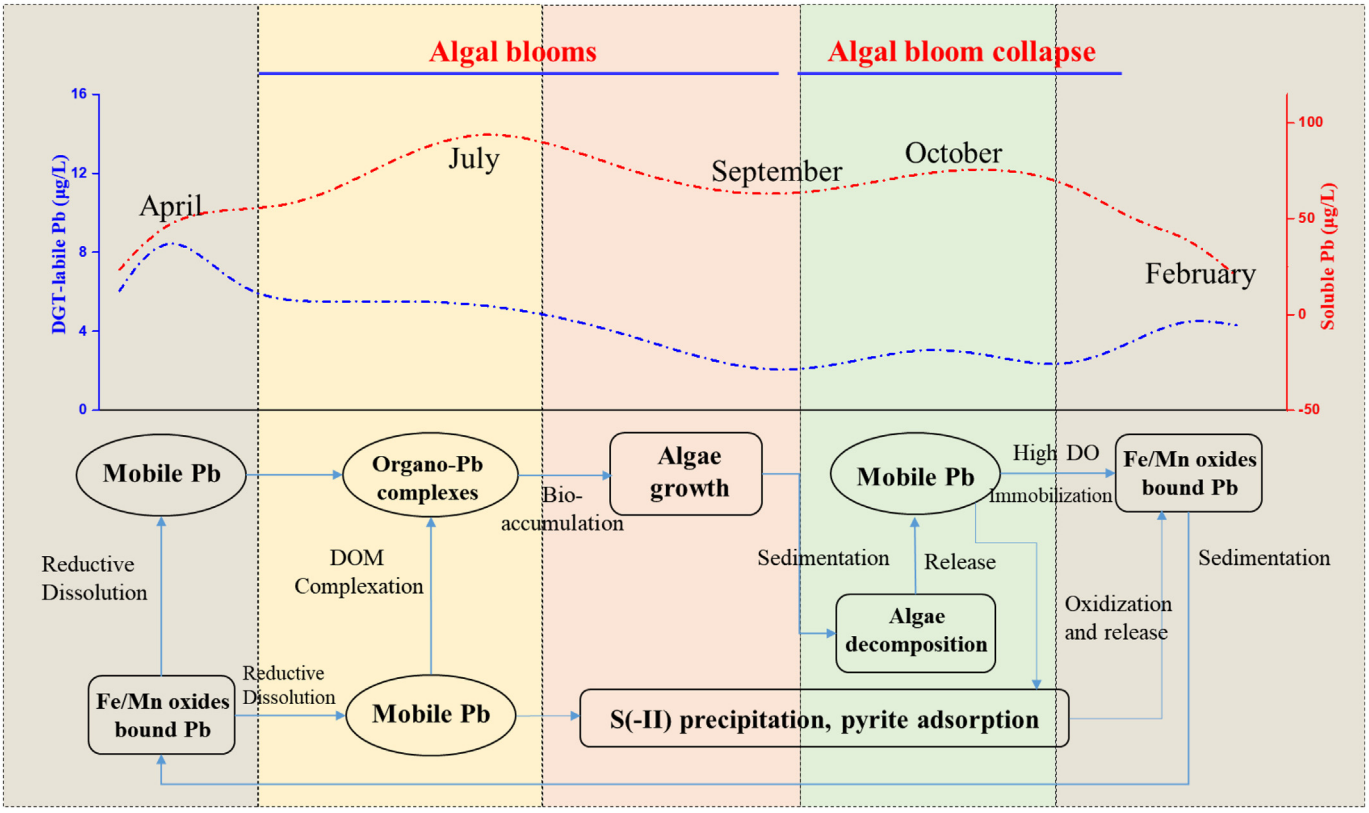

Fig. 9. The mechanism illustration for mobile Pb variation in overlying water-sediment system.

release of Pb in sediments to the water column from August through October. In winter months, elevated DO in overlying water and Eh in the sediment (Tables S1 and S2) will lead to acid volatile sulfide (AVS) and pyrite oxidation in surface sediment layers, resulting in the release of Pb (De Jonge et al., 2012; Wang et al., 2018). Released Pb will be in turn immobilized by Fe/Mn oxides, as reflected in December through February by the relatively low concentrations of dissolved (Figs. 3 and 4a).

4.3. Conclusion and implications

This study presented a full-year variation in mobile Pb concentrations in Meiliang Bay and revealed the corresponding mechanisms responsible for Pb mobilization. A mechanistic illustration of the monthly mobile Pb variation is shown in Fig. 9. It can be concluded that algal blooms significantly enhanced the mobilization of Pb in sediments and its release to the overlying water. Similarly, Yan et al. (2016) and Jin et al. (2019) reported that the concentrations of other metal (liod)s, such as zinc and high-toxic arsenic, were increased in hypereutrophic lakes during algal blooms. This study, together with the previous studies (Ni et al., 2016; Yan et al., 2016), demonstrated that the metal pollution in water can be increased by algal blooms through promoting the release of deposited/immobilized metals from sediments. The accumulation of Pb in the water column can in turn stimulate the aggregation of algal cells and contribute to the occurrence of algal blooms (Rzymski et al., 2014). Accordingly, continuous and dynamic interactions between algal blooms and sediment-released potentially toxic elements pose more serious threats to living organisms or even human health through bioaccumulation and biomagnification. Since Lake Taihu is a typical eutrophic lake with intensive cyanobacterial blooms, the results of this study provided valuable materials on assessing and interpreting metal contamination in other eutrophic lakes. It should be noted the Pb mobilization processes are much complicated in the field, and more direct evidences (e.g., Pb speciation in solids and pore waters) should be collected to support the interpretation of the relevant mechanisms obtained in this study using nondestructive techniques, such as X-ray absorption spectroscopy.

Acknowledgments

This study was jointly sponsored by the National Science Foundation of China (51879083, 41571465, 41621002), Research instrument and equipment Development Project of the Chinese Academy of Sciences (YJKYYQ20170016), CAS Interdisciplinary Innovation Team, “One-Three-Five” Strategic Planning of Nanjing Institute of Geography and Limnology (NIGLAS2017GH05), and a fund from the Priority Academic Program Development of Jiangsu Higher Education Institutions (PAPD).

Appendix A. Supplementary data

Supplementary data to this article can be found online at https://doi.org/10.1016/j.scitotenv.2019.07.152.

References

Banks, J.L., Ross, D.J., Keough, M.J., Eyre, B.D., Macleod, C.K., 2012. Measuring hypoxia induced metal release from highly contaminated estuarine sediments during a 40 day laboratory incubation experiment. Sci. Total Environ. 420, 229–237.

Baptista, M.S., Vasconcelos, V.M., Vasconcelos, M., 2014. Trace metal concentration in a temperate freshwater reservoir seasonally subjected to blooms of toxin-producing cyanobacteria. Microb. Ecol. 68, 671–678.

Cai, M.F., McBride, M.B., Li, K.M., Li, Z., 2017. Bioaccessibility of As and Pb in orchard and urban soils amended with phosphate, Fe oxide and organic matter. Chemosphere 173, 153–159.

Chakraborty, N., Banerjee, A., Pal, R., 2011. Accumulation of lead by free and immobilized cyanobacteria with special reference to accumulation factor and recovery. Bioresour. Technol. 102, 4191–4195.

Chakraborty, P., Chakraborty, S., Jayachandran, S., Madan, R., Sarkar, A., Linsy, P., Nath, B.N., 2016. Effects of bottom water dissolved oxygen variability on copper and lead fractionation in the sediments across the oxygen minimum zone, western continental margin of India. Sci. Total Environ. 566, 1052–1061.

Chen, M.S., Ding, S.M., Chen, X., Sun, Q., Fan, X.F., Lin, J., Ren, M.Y., Yang, L.Y., Zhang, C.S., 2018. Mechanisms driving phosphorus release during algal blooms based on hourly changes in iron and phosphorus concentrations in sediments. Water Res. 133, 153–164.

Chen, M., Ding, S., Lin, J., Fu, Z., Tang, W., Fan, X., Gong, M., Wang, Y., 2019. Seasonal changes of lead mobility in sediments in algae- and macrophyte-dominated zones of the lake. Sci. Total Environ. 660, 484–492.

De Jonge, M., Teuchies, J., Meire, P., Blust, R., Bervoets, L., 2012. The impact of increased oxygen conditions on metal-contaminated sediments part I: effects on redox status, sediment geochemistry and metal bioavailability. Water Res. 46, 2205–2214.

Del Giudice, D., Zhou, Y.T., Sinha, E., Michalak, A.M., 2018. Long-term phosphorus loading and springtime temperatures explain interannual variability of hypoxia in a large temperate lake. Environ. Sci. Technol. 52, 2046–2054.

DeVolder, P.S., Brown, S.L., Hesterberg, D., Pandya, K., 2003. Metal bioavailability and speciation in a wetland tailings repository amended with biosolids compost, wood ash, and sulfate. J. Environ. Qual. 32, 851–864.

Ding, S.M., Sun, Q., Xu, D., Jia, F., He, X., Zhang, C.S., 2012. High-resolution simultaneous measurements of dissolved reactive phosphorus and dissolved sulfide: the first observation of their simultaneous release in sediments. Environ. Sci. Technol. 46, 8297–8304.

Ding, S.M., Han, C., Wang, Y.P., Yao, L., Wang, Y., Xu, D., Sun, Q., Williams, P.N., Zhang, C.S., 2015. In situ, high-resolution imaging of labile phosphorus in sediments of a large eutrophic lake. Water Res. 74, 100–109.

Ding, S.M., Chen, M., Gong, M., Fan, X., Qin, B., Xu, H., Gao, S., Jin, Z., Tsang, D.C.W., Zhang, C., 2018. Internal phosphorus loading from sediments causes seasonal nitrogen limitation for harmful algal blooms. Sci. Total Environ. 625, 872–884.

Fu, J., Hu, X., Tao, X.C., Yu, H.X., Zhang, X.W., 2013. Risk and toxicity assessments of heavy metals in sediments and fishes from the Yangtze River and Taihu Lake, China. Chemosphere 93, 1887–1895.

Garcia-Hernandez, J., Garcia-Rico, L., Jara-Marini, M.E., Barraza-Guardado, R., Weaver, A.H., 2005. Concentrations of heavy metals in sediment and organisms during a harmful algal bloom (HAB) at Kun Kaak Bay, Sonora, Mexico. Mar. Pollut. Bull. 50, 733–739.

Garcia-Leston, J., Mendez, J., Pasaro, E., Laffon, B., 2010. Genotoxic effects of lead: an updated review. Environ. Int. 36, 623–636.

Han, C., Ding, S.M., Yao, L., Shen, Q.S., Zhu, C.G., Wang, Y., Xu, D., 2015. Dynamics of phosphorus-iron-sulfur at the sediment-water interface influenced by algae blooms decomposition. J. Hazard. Mater. 300, 329–337.

Hashimoto, Y., Takaoka, M., Oshita, K., Tanida, H., 2009a. Incomplete transformations of Pb to pyromorphite by phosphate-induced immobilization investigated by X-ray absorption fine structure (XAFS) spectroscopy. Chemosphere 76, 616–622.

Hashimoto, Y., Taki, T., Sato, T., 2009b. Extractability and leachability of Pb in a shooting range soil amended with poultry litter ash: investigations for immobilization potentials. J. Environ. Sci. Health A Tox. Hazard. Subst. Environ. Eng. 44, 583–590.

Hill, N.A., Simpson, S.L., Johnston, E.L., 2013. Beyond the bed: effects of metal contamination on recruitment to bedded sediments and overlying substrata. Environ. Pollut. 173, 182–191.

Howard, J.L., Vandenbrink, W.J., 1999. Sequential extraction analysis of heavy metals in sediments of variable composition using nitrilotriacetic acid to counteract resorption. Environ. Pollut. 106, 285–292.

Jin, Z.F., Ding, S.M., Sun, Q., Gao, S.S., Fu, Z., Gong, M.D., Lin, J., Wang, D., Wang, Y., 2019. High resolution spatiotemporal sampling as a tool for comprehensive assessment of zinc mobility and pollution in sediments of a eutrophic lake. J. Hazard. Mater. 364, 182–191.

Kumar, K.S., Dahms, H.U., Won, E.J., Lee, J.S., Shin, K.H., 2015. Microalgae - a promising tool for heavy metal remediation. Ecotoxicol. Environ. Saf. 113, 329–352.

Kushwaha, A., Hans, N., Kumar, S., Rani, R., 2018. A critical review on speciation, mobilization and toxicity of lead in soil microbe-plant system and bioremediation strategies. Ecotoxicol. Environ. Saf. 147, 1035–1045.

Leao, P.N., Vasconcelos, M., Vasconcelos, V.M., 2007. Role of marine cyanobacteria in trace metal bioavailability in seawater. Microb. Ecol. 53, 104–109.

Lezcano, M.A., Velazquez, D., Quesada, A., El-Shehawy, R., 2017. Diversity and temporal shifts of the bacterial community associated with a toxic cyanobacterial bloom: an interplay between microcystin producers and degraders. Water Res. 125, 52–61.

Li, C., Ding, S., Yang, L., Wang, Y., Ren, M., Chen, M., Fan, X., Lichtfouse, E., 2019. Diffusive gradients in thin films: devices, materials and applications. Environ. Chem. Lett. 17, 801–831.

Lu, R.K., 1999. Methods for Analysis of Soil Agrochemistry. Chinese Agriculture Science and Technology Press, Beijing.

Nemati, K., Abu Bakar, N.K., Abas, M.R., Sobhanzadeh, E., 2011. Speciation of heavy metals by modified BCR sequential extraction procedure in different depths of sediments from Sungai Buloh, Selangor, Malaysia. J. Hazard. Mater. 192, 402–410.

Ni, L.X., Li, D.D., Su, L.L., Xu, J.J., Li, S.Y., Ye, X., Geng, H., Wang, P.F., Li, Y., Li, Y.P., Acharya, K., 2016. Effects of algae growth on cadmium remobilization and ecological risk in sediments of Taihu Lake. Chemosphere 151, 37–44.

Niu, Y., Jiao, W., Yu, H., Niu, Y., Pang, Y., Xu, X.Y., Guo, X.C., 2015. Spatial evaluation of heavy metals concentrations in the surface sediment of Taihu Lake. Int. J. Environ. Res. Public Health 12, 15028–15039.

Ozverdi, A., Erdem, M., 2006. Cu^{2+}, Cd^{2+} and Pb^{2+} adsorption from aqueous solutions by pyrite and synthetic iron sulphide. J. Hazard. Mater. 137, 626–632.

Patel, P., Raju, N.J., Reddy, B.C.S.R., Suresh, U., Sankar, D.B., Reddy, T.V.K., 2018. Heavy metal contamination in river water and sediments of the Swarnamukhi River Basin, India: risk assessment and environmental implications. Environ. Geochem. Health 40, 609–623.

Pepi, M., Borra, M., Tamburrino, S., Saggiomo, M., Viola, A., Biffali, E., Balestra, C., Sprovieri, M., Casotti, R., 2016. A Bacillus sp isolated from sediments of the Sarno River mouth, Gulf of Naples (Italy) produces a biofilm biosorbing Pb(II). Sci. Total Environ. 562, 588–595.

Rajeshkumar, S., Liu, Y., Zhang, X.Y., Ravikumar, B., Bai, G., Li, X.Y., 2018. Studies on seasonal pollution of heavy metals in water, sediment, fish and oyster from the Meiliang Bay of Taihu Lake in China. Chemosphere 191, 626–638.

Rzymski, P., Poniedzialek, B., Niedzielski, P., Tabaczewski, P., Wiktorowicz, K., 2014. Cadmium and lead toxicity and bioaccumulation in Microcystis aeruginosa. Front. Environ. Sci. Eng. 8, 427–432.

Santner, J., Larsen, M., Kreuzeder, A., Glud, R.N., 2015. Two decades of chemical imaging of solutes in sediments and soils - a review. Anal. Chim. Acta 878, 9–42.

Sauve, S., McBride, M., Hendershot, W., 1998. Soil solution speciation of lead(II): effects of organic matter and pH. Soil Sci. Soc. Am. J. 62, 618–621.

Tack, F.M.G., Van Ranst, E., Lievens, C., Vandenberghe, R.E., 2006. Soil solution Cd, Cu and Zn concentrations as affected by short-time drying or wetting: the role of hydrous oxides of Fe and Mn. Geoderma 137, 83–89.

Tamura, H., Goto, K., Yotsuyan, T., Nagayama, M., 1974. Spectrophotometric determination of iron(II) with 1,10-phenanthroline in presence of large amounts of iron(III). Talanta 21, 314–318.

Tue-Ngeun, O., Sandford, R.C., Jakmunee, J., Grudpan, K., McKelvie, I.D., Worsfold, P.J., 2005. Determination of dissolved inorganic carbon (DIC) and dissolved organic carbon (DOC) in freshwaters by sequential injection spectrophotometry with on-line UV photo-oxidation. Anal. Chim. Acta 554 (1–2), 17–24.

Wang, S.L., Mulligan, C.N., 2008. Speciation and surface structure of inorganic arsenic in solid phases: a review. Environ. Int. 34, 867–879.

Wang, S.G., Diao, X.J., He, L.S., 2015. Effects of algal bloom formation, outbreak, and extinction on heavy metal fractionation in the surficial sediments of Chaohu Lake. Environ. Sci. Pollut. Res. 22, 14269–14279.

Wang, C., Bai, L., Jiang, H., Xu, H.C., 2016a. Algal bloom sedimentation induces variable control of lake eutrophication by phosphorus inactivating agents. Sci. Total Environ. 557, 479–488.

Wang, Y., Ding, S.M., Gong, M.D., Xu, S.W., Xu, W.M., Zhang, C.S., 2016b. Diffusion characteristics of agarose hydrogel used in diffusive gradients in thin films for measurements of cations and anions. Anal. Chim. Acta 945, 47–56.

Wang, Y., Ding, S.M., Shi, L., Gong, M.D., Xu, S.W., Zhang, C.S., 2017. Simultaneous measurements of cations and anions using diffusive gradients in thin films with a ZrO-Chelex mixed binding layer. Anal. Chim. Acta 972, 1–11.

Wang, S.R., Wu, Z.H., Luo, J., 2018. Transfer mechanism, uptake kinetic process, and bioavailability of P, Cu, Cd, Pb, and Zn in macrophyte rhizosphere using diffusive gradients in thin films. Environ. Sci. Technol. 52, 1096–1108.

Wolfe, A.L., Wilkin, R.T., 2017. Evidence of sulfate-dependent anaerobic methane oxidation within an area impacted by coalbed methane-related gas migration. Environ. Sci. Technol. 51, 1901–1909.

Xu, D., Wu, W., Ding, S.M., Sun, Q., Zhang, C.S., 2012. A high-resolution dialysis technique for rapid determination of dissolved reactive phosphate and ferrous iron in pore water of sediments. Sci. Total Environ. 421, 245–252.

Xu, H., Paerl, H.W., Zhu, G.W., Qin, B.Q., Hall, N.S., Zhu, M.Y., 2017. Long-term nutrient trends and harmful cyanobacterial bloom potential in hypertrophic Lake Taihu, China. Hydrobiologia 787, 229–242.

Yan, C.Z., Che, F.F., Zeng, L.Q., Wang, Z.S., Du, M.M., Wei, Q.S., Wang, Z.H., Wang, D.P., Zhen, Z., 2016. Spatial and seasonal changes of arsenic species in Lake Taihu in relation to eutrophication. Sci. Total Environ. 563, 496–505.

Yang, Z., Zhang, M., Shi, X.L., Kong, F.X., Ma, R.H., Yu, Y., 2016. Nutrient reduction magnifies the impact of extreme weather on cyanobacterial bloom formation in large shallow Lake Taihu (China). Water Res. 103, 302–310.

Yang, Y., Chen, T.H., Sumona, M., Sen Gupta, B., Sun, Y.B., Hu, Z.H., Zhan, X.M., 2017. Utilization of iron sulfides for wastewater treatment: a critical review. Rev. Environ. Sci. Biotechnol. 16, 289–308.

Yao, X., Zhang, Y.L., Zhu, G.W., Qin, B.Q., Feng, L.Q., Cai, L.L., Gao, G.A., 2011. Resolving the variability of CDOM fluorescence to differentiate the sources and fate of DOM in Lake Taihu and its tributaries. Chemosphere 82, 145–155.

Yin, H.B., Fan, C.X., Ding, S.M., Zhang, L., Li, B., 2008. Acid volatile sulfides and simultaneously extracted metals in a metal-polluted area of Taihu Lake, China. Bull. Environ. Contam. Toxicol. 80, 351–355.

Yin, H.B., Gao, Y.N., Fan, C.X., 2011. Distribution, sources and ecological risk assessment of heavy metals in surface sediments from Lake Taihu, China. Environ. Res. Lett. 6, 11.

Zohar, I., Bookman, R., Levin, N., de Stigter, H., Teutsch, N., 2014. Contamination history of lead and other trace metals reconstructed from an urban winter pond in the Eastern Mediterranean Coast (Israel). Environ. Sci. Technol. 48, 13592–13600.